

Characterizing Attribute Distributions in Water Sediments by Geostatistical Downscaling

YUNTAO ZHOU[†] AND
ANNA M. MICHALAK^{*,†,‡}

Department of Civil and Environmental Engineering, and
Department of Atmospheric, Oceanic and Space Sciences,
University of Michigan, Ann Arbor, Michigan 48109

Received May 13, 2009. Revised manuscript received
September 10, 2009. Accepted October 12, 2009.

Information about attributes such as contaminant concentrations or hydraulic properties in benthic sediments is typically obtained in core sections of varying lengths, and only the average value is measured in each section. However, an estimate of the attribute distribution at a uniform spatial resolution is often required for site characterization and the design of appropriate risk-based remediation alternatives. Because attributes exhibit spatial autocorrelation, geostatistical methods have become an essential tool for estimating their spatial distribution. The purpose of this paper is to optimally infer the spatial distribution of sampled attributes at a uniform resolution from fluvial core sampling data, using a downscaling technique formulated as a geostatistical inverse problem. We compare geostatistical downscaling to the more traditional approach of point-to-point ordinary kriging for a hypothetical case study, and for total organic carbon observations from the Passaic River, New Jersey. Although frequently used to interpolate measurements, ordinary kriging is shown not to be able to estimate the spatial distribution of attributes accurately, because this approach assumes that data are sampled at a uniform resolution. Geostatistical downscaling, on the other hand, is shown to resolve this problem by explicitly accounting for the relationship between the known average measurements and the unknown fine-resolution attribute distribution to be estimated.

1. Introduction

Remediation of contaminated fluvial or lake sediments is costly (1, 2), and often requires detailed knowledge of the distribution of contamination in the subsurface to formulate effective remediation strategies (1, 3). Measuring spatially distributed attributes important for remediation (e.g., contaminant concentrations or hydraulic properties) everywhere in a system is not practical or cost-effective, however. Thus, knowledge of subsurface properties is often limited to a set of incomplete information obtained from sparse sampling. Due to the irregular thickness of sediment above the bedrock surface, samples of contaminated stream or riverbed sediments are often obtained from cores that vary in length. Each core is subsequently subdivided into several sections of varying thickness, which are analyzed for key attributes (e.g., Figure 1b). The reported values at each location typically

represent an average within individual segments of each core, and the sampling resolution (aka support) is therefore nonuniform.

While beneficial for qualitative site characterization, measured average parameter values from sparse sampling provide insufficient detail about the spatial distribution of the attributes throughout the sampled area for purposes of remediation design and assessment. Therefore, interpolation methods, including geostatistical methods, mathematical splines, and inverse distance weighted interpolation (4–6), are typically used to map the attribute distribution throughout the site. Given that the sampled attributes often exhibit spatial continuity (3), geostatistical methods, which explicitly account for spatial autocorrelation, are common (3, 7, 8). In addition to an estimate of the distribution of the attribute, geostatistical methods also provide a measure of the uncertainty associated with the interpolated values (9).

The direct application of traditional geostatistical tools for data with nonuniform resolution, as is typical of data sets describing contaminated sediments, is problematic for several reasons, however. First, a uniform resolution is required by a majority of interpolation approaches, including those that fall within the framework of geostatistical interpolation (e.g., point-to-point ordinary kriging). To apply such tools, one needs to make some assumptions regarding the distribution of the attribute within the individual core sections. In general, this is done by performing the spatial interpolation at a resolution finer than the resolution of the core sections, and assuming either (i) that the sampled average value is representative of the attribute value at the center of each original section, or (ii) that the measured average value is representative of the attribute value at every point in the core section (3). Violating the requirement for uniform measurement resolution in this way can yield inaccuracies in both the estimated field and its associated estimation error, as will be demonstrated in the applications presented in this paper. Second, the variance of a spatially distributed attribute usually varies with the spatial resolution of measurements (10), with apparent variance usually decreasing with coarser resolution, while the converse is true with correlation lengths (11). Therefore, accurate information about the data structure at the resolution of the final estimates, including a measure of overall variability and correlation length that are required for geostatistical analysis, is difficult to obtain using a data set with variable resolution. When data with variable resolution are used for estimating variability, the true variability can be underestimated due to the averaging process inherent to sampling in nonuniform core sections.

Estimating attribute values at a finer, uniform resolution (i.e., downscaling) is an option for solving the mixed-resolution problem. Downscaling in a geostatistical cokriging framework has been successfully applied in past studies (12), but requires the joint estimation of multiple attributes. Alternately, this paper presents a geostatistical downscaling approach, expressed as a special form of a linear geostatistical inverse problem, which can account for variable resolution in the data. Geostatistical inverse modeling has been widely used in hydrogeology for characterizing contaminant sources (13–15) and identifying the distribution of hydraulic conductivities or transmissivities in aquifers (16–18). In this work, geostatistical downscaling is applied to benthic sediment data, through the definition of a sensitivity matrix representing the quantitative relationship between the measured average attribute value and the uniform resolution values to be estimated. The downscaling approach is similar to the

* Corresponding author phone: 734-763-9664; fax: 734-763-2275; e-mail: amichala@umich.edu.

[†] Department of Civil and Environmental Engineering.

[‡] Department of Atmospheric, Oceanic and Space Sciences.

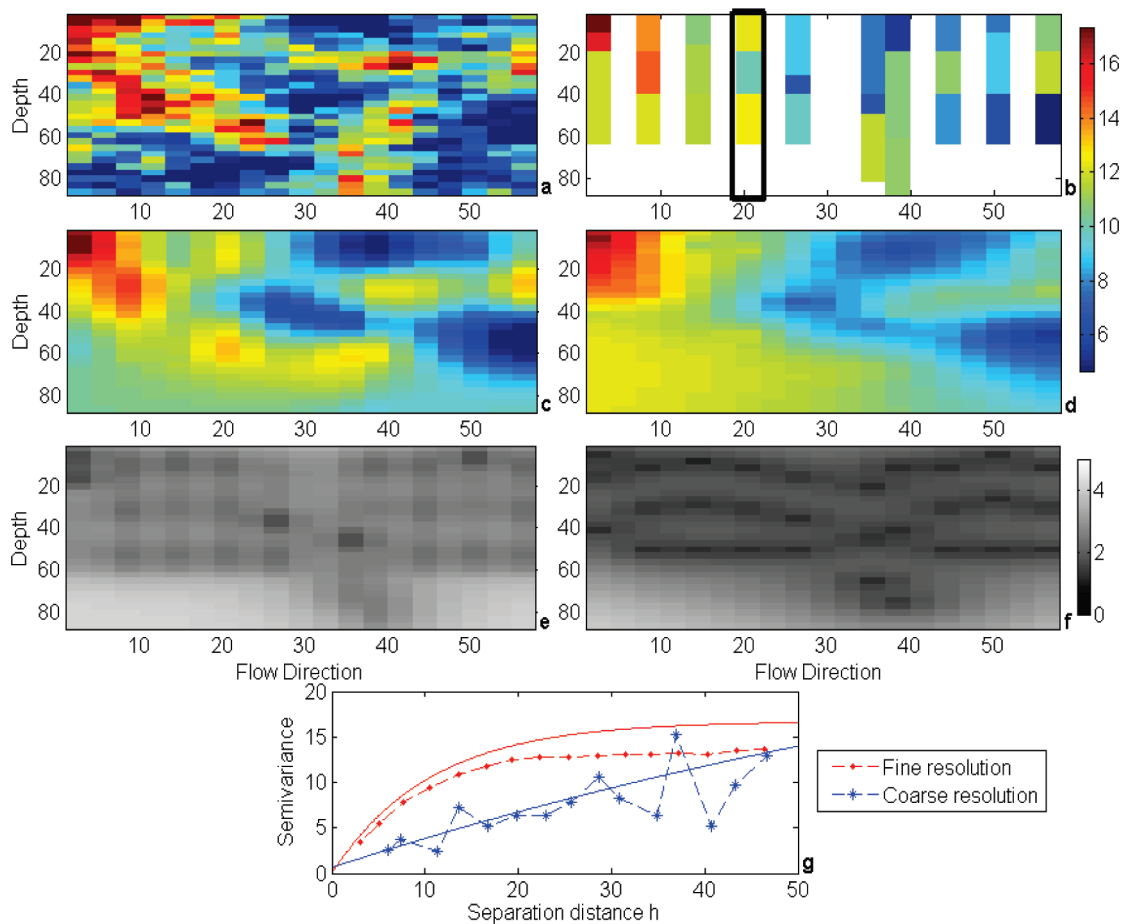


FIGURE 1. Data and estimates for pseudodata example: (a) fine-resolution attribute distribution; (b) available coarse-resolution (average) data; (c) GD best estimates; (d) OK best estimates; (e) GD estimation uncertainty standard deviation; (f) OK estimation uncertainty standard deviation; (g) experimental (dashed lines) and theoretical (solid lines) variograms. The coarse-resolution experimental variogram (blue dashed) was derived using available data in (b). The fine-resolution experimental variogram (red dashed) was derived using the true fine-resolution data in (a). Both theoretical variograms were derived using REML and the data in (b).

area-to-point kriging approach presented in Kyriakidis (19) for interpolating point values from available areal data, which accounts for the linear average constraint to the areal data. The approach presented here is similar, but also allows for the covariance parameters to be estimated directly from available multiresolution data. Because the presented approach does not assume a uniform resolution for the sampled data, it preserves the true, underlying, variability of the sampled attributes during the downscaling process.

The primary objective of this paper is to investigate the potential advantages of implementing a geostatistical downscaling method for inferring sediment attribute values at a consistent resolution, using data from variable-resolution core sections.

2. Methods

2.1. Initial Setup for Geostatistical Downscaling. The geostatistical downscaling (GD) approach is formulated as a geostatistical inverse problem, in which the forward model refers to the process of estimating average observations at the sampled resolution from attribute values defined at a (finer) uniform resolution, while the inverse problem involves the estimation of attribute values at a uniform distribution given sampled values representative of variable-depth increments. Detailed descriptions of linear geostatistical inverse modeling (GIM) are available in Snodgrass and Kitanidis (15) and Michalak et al. (20), among others, and only the key equations are reproduced here.

Linear GIM assumes a linear relationship between the field (\mathbf{s}) to be estimated and the available measurements (\mathbf{z}):

$$\mathbf{z} = \mathbf{H}\mathbf{s} + \mathbf{v} \quad (1)$$

where \mathbf{z} is an $n \times 1$ vector of observations (in this case, average concentrations or weight percents) and \mathbf{s} is an $m \times 1$ vector of unknown attribute values at a uniform resolution. The measurement errors \mathbf{v} are modeled as an $n \times 1$ vector of independent, normally distributed random variables with zero mean and variance $\sigma_{\mathbf{R}}^2$. Hence, the $n \times n$ covariance matrix \mathbf{R} of \mathbf{v} is:

$$\mathbf{R} = \sigma_{\mathbf{R}}^2 \mathbf{I}_z \quad (2)$$

where \mathbf{I}_z is an $n \times n$ identity matrix. This measurement error variance is estimated using the kriging setup as described in Section 2.2. The known $n \times m$ matrix \mathbf{H} (where $H_{ij} = \partial z_i / \partial s_j$) describes the linear averaging relationship between measurements \mathbf{z} and estimated attribute values \mathbf{s} . In the case examined here, \mathbf{H} is

$$H_{ij} = \begin{cases} \frac{1}{N_i}, & d_{U_i} < d_j < d_{L_i} \\ 0, & \text{otherwise} \end{cases} \quad (3)$$

where N_i is the number of fine-resolution estimation locations contained in the i^{th} measured core section, d_j is the depth of estimation location j , and d_{U_i} and d_{L_i} are the upper and

lower boundaries of the core section corresponding to measurement i , respectively.

The unknown field \mathbf{s} is modeled as a random vector with expected value

$$E[\mathbf{s}] = \mathbf{X}_s \beta_s \quad (4)$$

where \mathbf{X}_s defines known zonation (18) or spatial trends of \mathbf{s} (15). For this work, we assume that the attribute value in the sediment has a constant but unknown mean β_s , and \mathbf{X}_s therefore becomes an $m \times 1$ vector of ones.

The spatial autocorrelation of the estimated field is modeled using an $m \times m$ covariance matrix \mathbf{Q}_{ss} , which describes the correlation structure of deviations of \mathbf{s} from the mean:

$$E[(\mathbf{s} - \mathbf{X}_s \beta_s)(\mathbf{s} - \mathbf{X}_s \beta_s)^T] = \mathbf{Q}_{ss}(\boldsymbol{\theta}_s) \quad (5)$$

where T indicates a transpose, and $\boldsymbol{\theta}_s$ are structural parameters required for defining the covariance function at the resolution of the estimates. In the cases that will be examined in Section 2.3,

$$\boldsymbol{\theta}_s = \{\sigma^2, l_f, l_v, \sigma_Q^2\} \quad (6)$$

where σ^2 is the variance, at the fine-scale resolution, of the portion of the attribute variability that is spatially correlated, σ_Q^2 is the microscale variability (i.e., the portion of the variability that is not spatially correlated), and l_f and l_v are the correlation range parameters along the flow and vertical directions for the 2D applications. If the field data display anisotropy, then l_f and l_v will be different. Overall, the covariance function describing the spatial autocorrelation of the estimated attribute is assumed to follow an exponential model combined with nugget effect, based on an examination of the data from the Passaic River, as will be further described in Section 2.3:

$$\mathbf{Q}_{ss}(\mathbf{h}|\boldsymbol{\theta}_s) = \sigma^2 \exp\left(-\sqrt{\left(\frac{\mathbf{h}_f}{l_f}\right)^2 + \left(\frac{\mathbf{h}_v}{l_v}\right)^2}\right) + \sigma_Q^2 \cdot \mathbf{I}_s \quad (7)$$

where \mathbf{h}_f and \mathbf{h}_v are the matrices of separation distances, along the flow and vertical directions, respectively, between any two estimation locations, and \mathbf{I}_s is an $m \times m$ identity matrix. As is clear from eq 7, the total variance is $\sigma^2 + \sigma_Q^2$. The corresponding variogram, which represents dissimilarities between pairs of values, is:

$$\gamma_s(\mathbf{h}|\boldsymbol{\theta}_s) = \sigma^2 \left(1 - \exp\left(-\sqrt{\left(\frac{\mathbf{h}_f}{l_f}\right)^2 + \left(\frac{\mathbf{h}_v}{l_v}\right)^2}\right)\right) + \sigma_Q^2 \left(1 - \delta[\sqrt{\mathbf{h}_f^2 + \mathbf{h}_v^2}]\right) \quad (8)$$

where $\delta[\]$ is a Kronecker delta function, equal to one when the separation distance is zero. The parameters used in eqs 6–8 are optimized using a Restricted Maximum Likelihood (REML) approach (21) from the available variable-resolution data, as will be described in Section 2.3. Once all relevant vectors and matrices have been defined, the GD estimation problem is set up as described in Section 2.4.

2.2. Initial Setup for Ordinary Kriging. Point-to-point ordinary kriging (OK) has been used extensively for parameter interpolation. In contrast to GD, it requires the data to have the same resolution at each measurement and estimation location within the entire domain (10). Therefore, if OK is used for interpolation, all observations must be assumed to have uniform resolution. To achieve this goal for sediment data involving variable core section thicknesses, the sections are divided into uniform subsections, and the measured value in the core section is assumed to represent the value at the

center of the section. Hence, the spatial covariance structure of the fine-resolution estimates and variable-resolution measurements are implicitly assumed to be the same. In the presented OK applications (used for comparison), the portion of the observed variability that is not spatially correlated is assumed to be due to measurement errors, and OK is implemented in the continuous part kriging (aka kriging with measurement error) form (10, 22).

In this setup, the covariance of the measurements is:

$$\mathbf{Q}_{zz}(\mathbf{h}|\boldsymbol{\theta}_z) = \sigma^2 \exp\left(-\sqrt{\left(\frac{\mathbf{h}_f}{l_f}\right)^2 + \left(\frac{\mathbf{h}_v}{l_v}\right)^2}\right) + \sigma_R^2 \cdot \mathbf{I}_z \quad (9)$$

where $\boldsymbol{\theta}_z$ are covariance parameters obtained directly from the available observations, and all other parameters are as defined in Section 2.1, except that \mathbf{h}_f and \mathbf{h}_v are now $n \times n$ matrices, because they refer to the measurement locations, and \mathbf{I}_z is an $n \times n$ identity matrix. Note also that the uncorrelation portion of the variability is designated σ_R^2 , due to the assumption that this variability is caused by measurement errors. The structural parameters in the OK formulation are:

$$\boldsymbol{\theta}_z = \{\sigma^2, l_f, l_v, \sigma_R^2\} \quad (10)$$

REML is used to estimate the parameters of the covariance matrix (\mathbf{Q}_{zz}), as described in Section 2.3. The system of equations for OK is presented in Section 2.4.

2.3. Covariance Parameter Optimization. There are many approaches for estimating the covariance parameters required for the application of geostatistical methods, including least-squares fits to observed variability (23), maximum likelihood methods (24–26), REML (15, 21), composite likelihood (27), and generalized estimation equations (27). REML is used in this work because this approach is applicable to both GD and OK, and because it has been shown to limit the bias in the estimated covariance parameters (24).

The REML approach maximizes the likelihood of available observations after marginalizing with respect to the unknown drift coefficient β (15, 21). For GD, this is equivalent to minimizing the following objective function:

$$I_{\theta, \text{GD}} = \frac{1}{2} \ln|\Omega| + \frac{1}{2} \ln|\mathbf{X}_s^T \mathbf{H}^T \Omega^{-1} \mathbf{H} \mathbf{X}_s| + \frac{1}{2} \mathbf{z}^T \Xi_{\text{GD}} \mathbf{z} \quad (11)$$

$$\Omega = \mathbf{H} \mathbf{Q}_{ss} \mathbf{H}^T + \mathbf{R} \quad (12)$$

$$\Xi_{\text{GD}} = \Omega^{-1} - \Omega^{-1} \mathbf{H} \mathbf{X}_s (\mathbf{X}_s^T \mathbf{H}^T \Omega^{-1} \mathbf{H} \mathbf{X}_s)^{-1} \mathbf{X}_s^T \mathbf{H}^T \Omega^{-1} \quad (13)$$

where $|\ |$ denotes matrix determinant. The variance of the measurement errors (σ_R^2) is assumed the same as in the kriging application. For OK, the structural parameters in \mathbf{Q}_{zz} are obtained by minimizing the cost function:

$$I_{\theta, \text{OK}} = \frac{1}{2} \ln|\mathbf{Q}_{zz}| + \frac{1}{2} \ln|\mathbf{X}_z^T \mathbf{Q}_{zz}^{-1} \mathbf{X}_z| + \frac{1}{2} \mathbf{z}^T \Xi_{\text{OK}} \mathbf{z} \quad (14)$$

$$\Xi_{\text{OK}} = \mathbf{Q}_{zz}^{-1} - \mathbf{Q}_{zz}^{-1} \mathbf{X}_z (\mathbf{X}_z^T \mathbf{Q}_{zz}^{-1} \mathbf{X}_z)^{-1} \mathbf{X}_z^T \mathbf{Q}_{zz}^{-1} \quad (15)$$

where \mathbf{X}_z is an $n \times 1$ vector of ones. Note that eqs 11 and 14 are nonlinear with respect to the parameters in \mathbf{Q} . A simple unconstrained nonlinear optimization routine was implemented in this work, although more sophisticated gradient-based approaches can also be used (e.g. (15)).

2.4. Solution. Following the GD and OK setup as described in Sections 2.1 and 2.2, and after obtaining the covariance parameters as described in Section 2.3, the

TABLE 1. Parameters of Equation 16 Used for GD and OK

method	covariance of observations $\Sigma_{zz} (n \times n)$	covariance between observations and estimates $\Sigma_{zs} (n \times m)$	trend of observations $F_z (n \times 1)$	trend of estimates $F_s (m \times 1)$	covariance of estimates $\Sigma_{ss} (m \times m)$
OK	Q_{zz}	Q_{zs}	X_z	X_s	Q_{ss}
GD	$HQ_{ss}H^T + R$	HQ_{ss}	HX_s	X_s	Q_{ss}

solution for both GD and OK can be expressed as a special form of cokriging:

$$\begin{bmatrix} \Sigma_{zz} & F_z \\ F_z^T & 0 \end{bmatrix} \begin{bmatrix} \Lambda^T \\ M \end{bmatrix} = \begin{bmatrix} \Sigma_{zs} \\ F_s^T \end{bmatrix} \quad (16)$$

where the individual terms are as defined in Table 1, Σ_{zz} represents covariance between observations, Σ_{zs} represents the covariance between observation and estimation locations, F_z and F_s are the trends at measurement and estimation locations, Λ is an $m \times n$ matrix of optimized weights assigned to the available measurements, and M is a $1 \times m$ vector of Lagrange multipliers. Λ and M are estimated from eq 16. In Table 1, Q_{zs} is the covariance matrix between measurement and estimation locations without the measurement error (σ_R^2), Q_{ss} in OK is a covariance matrix that has the same parameters as Q_{zz} but represents the covariance between estimation locations.

The estimated attribute distribution and its associated uncertainty covariance matrix are defined as:

$$\hat{s} = \Lambda z \quad (17)$$

$$V_{\hat{s}} = -F_s M + \Sigma_{ss} - \Sigma_{zs}^T \Lambda^T \quad (18)$$

where \hat{s} is the best estimate at the uniform fine-scale resolution, and the square roots of the diagonal elements of $V_{\hat{s}}$ are the standard deviations of the estimation uncertainty.

3. Data Availability and Description

This section describes the two applications used to evaluate the GD approach. The first application is based on pseudodata generated to be representative of variability typically observed in contaminated river sediments. The second application uses total organic carbon (TOC) data from the Passaic River in New Jersey.

The data (Figure 1a) for the first application were generated at a fine, uniform resolution, using a prespecified spatial covariance matrix, and were then averaged to represent core sections of differing lengths (Figure 1b). For simplicity, the data were generated using an isotropic model, such that only one correlation range parameter l is required. These average observations were assumed known, and were used as the basis for recovering the original fine-resolution spatial distribution of the attribute and its associated spatial covariance parameters.

The field data used in the second application represent the sediment TOC weight percentage in a 10-km stretch of the lower Passaic River, acquired from the U.S. EPA (28) and a sediment database compiled by NOAA (29). A 2D section along the flow and vertical directions of the sediment bed is analyzed in this work, which includes 27 cores and a total of 153 core sections as measurements (Figure 3a), as well as over 5500 estimation locations (Figure 3b). The TOC measurements represent the average weight percent within the core sections, all of which are ≥ 30 cm long. Due to river meandering, the separation distance between two locations (h) is calculated as the shortest in-water path (8) to avoid including paths over the intervening land surfaces (3).

4. Results and Discussion

4.1. Pseudodata Application. The blue lines in Figure 1g present the experimental variogram (dashed line) obtained using the samples from Figure 1b, together with the theoretical variogram fit (solid line) based on the parameters estimated using the OK version of the REML algorithm (eq 14). The red lines in Figure 1g represent the experimental variogram (dashed line) at the estimation resolution (Figure 1a), and the theoretical variogram fit (solid line, eq 8) based on the parameters estimated using the GD version of the REML algorithm (eq 11). Only the available measurements presented in Figure 1b were used to obtain the theoretical

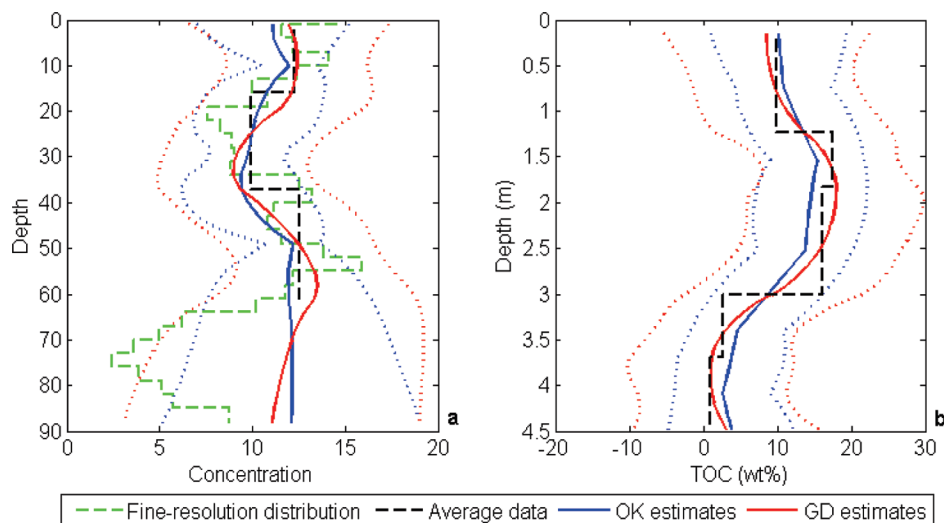


FIGURE 2. 1D slices of estimates for (a) pseudodata and (b) field data examples. The locations of the two slices are indicated with black frames in Figure 1b and Figure 3a, respectively. Solid lines represent best estimates. Dotted lines represent 95% confidence intervals. Note that the true fine-resolution distribution is unknown for the field data example.

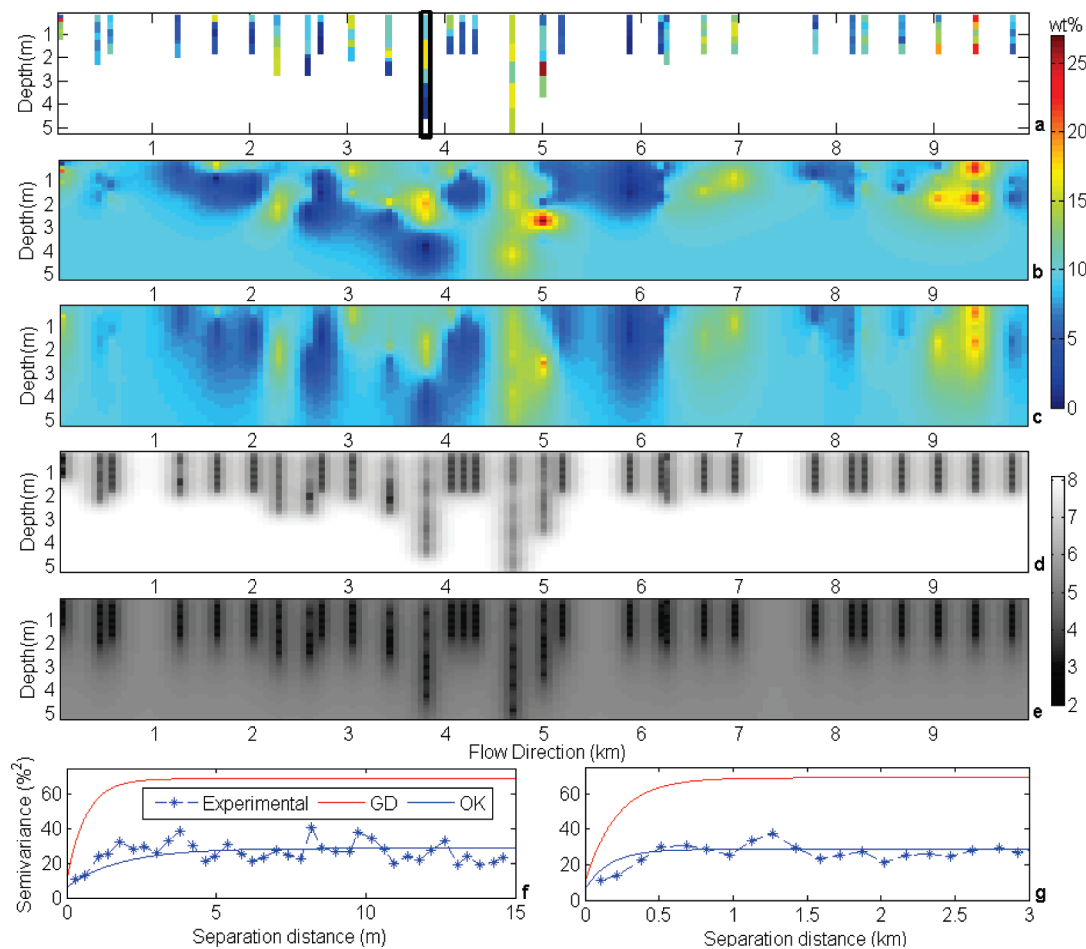


FIGURE 3. Data and estimates for field data TOC (a) available coarse-resolution (average) data; (b) GD best estimates; (c) OK best estimates; (d) GD estimation uncertainty standard deviation; (e) OK estimation uncertainty standard deviation; (f) experimental (dashed line) and theoretical (solid lines) variograms along vertical direction; (g) experimental (dashed line) and theoretical (solid lines) variograms along flow direction. The experimental variograms were derived using REML and the data in (a). All theoretical variograms were derived using REML and the data in (a).

(solid lines) variogram parameters at both resolutions. As illustrated by the two experimental variograms, the amount of variability in the available data is less than that at the fine-scale resolution. This is evident by the fact that the total variance is lower for the averaged observations, and the correlation length (which is the rate at which the variance approaches its maximum value as the separation distance increases) is longer. Because we are interested in estimating the attribute distribution at the uniform resolution illustrated in Figure 1a, it is the variability illustrated by the red dashed line that is the one we need to reproduce. Based on the two theoretical variograms, it is clear that the variogram based on an ordinary kriging setup reproduces the variability at the nonuniform observation resolution, and underestimates the variability at the target fine-scale resolution. Conversely, the theoretical variogram estimated using the GD setup of REML captures the variability at the fine-scale resolution, even though it is also based only on the available data at the coarser scale.

Figure 1c and d present the best estimates of the attribute distribution at the fine-scale resolution for GD and OK, respectively. Visually, it is clear that the best estimates from GD are closer to the fine-resolution pseudodata than those from OK. It is also clear that the OK best estimates show less variability when compared to GD. This can also be seen in Figure 2a, which shows a 1D vertical slice from the 2D results presented in Figure 1. Although neither of the applied interpolation methods can reproduce the true fine-resolution attribute distribution precisely due to the lack of fine-scale

observations, the GD results are much closer to the true distribution of fine-scale pseudodata, with the OK estimates showing insufficient variability.

Figure 1e and f present the estimation uncertainties associated with the GD and OK estimated attribute distribution (eq 18). A good uncertainty estimate is one that correctly quantifies the errors associated with the estimates from a particular method. Figure 2a also presents the upper and lower 95% uncertainty bounds for one vertical slice from the 2D results. As can be seen from Figures 1e and f and 2a, the uncertainty estimates from GD are higher relative to those from OK. Looking at the results presented in Figure 2a, however, it is clear that OK underestimates the uncertainty associated with its estimates. This can be seen from the fact that the true attribute distribution at the estimation scale (which is known because this case is a pseudodata application) lies outside of the uncertainty bounds for a large portion of the estimation locations. In the entire 2D domain, only 83.3% of true attribute values lie within two standard deviations of the OK estimates, whereas 96.7% of true values lie within two standard deviations of the GD estimates. Theoretically, 95% of true values should fall within these bounds. This indicates that although the uncertainties from OK are narrower, they do not adequately represent the true uncertainties of the fine-resolution estimates. Since OK assumes that the measured average attribute values are representative of variability at the finer estimation resolution, it underestimates variability at fine resolutions, leading to the observed underestimates of the estimation uncertainty.

Figure 1e and f also confirm that the uncertainty for both methods grows as the distance between the sampled cores and estimation locations increases, as would be expected. In addition, these figures and Figure 2a also suggest that the uncertainty from OK is lowest at the center of each core section, while the GD uncertainties within core sections are relatively uniform. This again reflects the different assumptions made by OK and GD about the location where the measurements reflect the true attribute value.

4.2. Field Application. Sediment TOC data are typically collected together with contaminant concentrations as part of ecological risk assessments (30). TOC forms water-soluble and water-insoluble complexes with metal ions and hydrous oxides, interacts with clay minerals, binds particles together, and sorbs and desorbs both naturally occurring and anthropogenically introduced organic contaminants (30). The analysis of the TOC distribution is therefore an essential component of the analysis of contaminant distributions. TOC data from the lower Passaic River (Figure 3a) are analyzed here, using the same tools applied for the pseudodata application in Section 4.1.

The blue lines in Figure 3f and g present the experimental variogram (dashed line) obtained using the samples from Figure 3a, together with the theoretical variogram fit (solid line) based on the parameters estimated using the OK version of the REML algorithm. The experimental variogram at the fine-scale resolution cannot be obtained in this case, because the attribute distribution at a fine resolution is unknown. However, the GD version of REML is used to derive the fine-scale variability. This approach was shown in Section 4.1 to yield a good representation of the true fine-scale variability. Based on the results from the pseudodata application, it is expected that the estimated variogram at the estimation scale would display more variability than the variogram at the measurement resolution, and this is indeed the case. Moreover, correlation lengths along the vertical direction (Figure 3f) from OK and GD were found to be much shorter than those along the flow direction (Figure 3g), which is consistent with earlier work (3).

Figure 3b and c present the best estimates of the attribute distribution at the fine-scale resolution for GD and OK. Consistent with the pseudodata example, it is clear from Figure 3 that the OK best estimates show less variability when compared to GD. This can also be seen in Figure 2b, which shows a 1D vertical slice from the 2D results presented in Figure 3. Although the "true" TOC distribution at the fine-scale resolution is not known in this case, the pseudodata example presented in Section 4.1 showed that the GD estimates are more representative of the expected variability at the fine-scale resolution. The significant differences between the OK (Figure 3c) and GD (Figure 3b) estimates confirm that explicitly accounting for scale differences has a large impact on the estimated spatial distribution of field attributes.

Figure 3d and e present the estimation uncertainties associated with the GD and OK. Figure 2b also presents the 95% uncertainty bounds for one vertical slice from the 2D results. The uncertainty estimates from the GD approach are again higher relative to those from OK. Because OK assumes that the measured average attribute values are representative of the variability at the finer estimation resolution, it underestimates the variability and the uncertainties at fine resolutions. This indicates that, although the estimated uncertainties from OK are lower, they cannot accurately represent the true uncertainties of the OK estimates. Note that, although not implemented here, a numerical approach such as a Gibbs sampling algorithm could be implemented to enforce nonnegativity in the uncertainty bounds (31).

The GD method presented in this paper provides a rigorous approach for using data sampled at a nonuniform resolution to characterize the spatial distribution of attributes in sediments. GD infers the degree of spatial variability at a target resolution, and uses this information, together with information about the resolution of individual available samples, to yield an estimate of the attribute distribution at the target resolution and its associated uncertainty. The pseudodata example demonstrated that the GD approach can more accurately represent the true degree of spatial variability in the underlying distribution, and yield better estimates with a more accurate assessment of uncertainties, relative to traditional OK. The field application confirms that these differences have an impact on estimates at the field scale. For the Passaic River application, the GD estimates of TOC suggest more continuity in the flow direction at this site relative to OK. In addition, the estimation uncertainty is very high in many areas of the domain, due to the uneven and sparse sampling in the field. The high uncertainties in Figure 3d indicate that the prediction precision is limited, and that additional sampling would be beneficial, especially along the flow direction.

Ongoing work is extending the approach presented here to parameters that exhibit skewed probability distributions, as is often the case, for example, with contaminant concentrations. While the application presented here involves water sediments, the methodology can also be adapted to other areas where sampling is conducted at multiple resolutions.

Acknowledgments

This work was supported by National Science Foundation award number 0644648, CAREER: Development of Geostatistical Data Assimilation Tools for Water Quality Monitoring. We thank Deborah Huntzinger for valuable feedback on this manuscript, and Noemi Barabás for providing field data and advice in the early stages.

Literature Cited

- Wang, Q. R.; Kim, D.; Dionysiou, D. D.; Sorial, G. A.; Timberlake, D. Sources and remediation for mercury contamination in aquatic systems - a literature review. *Environ. Pollut.* **2004**, *131*, 323-336.
- Wu, L. Review of 15 years of research on ecotoxicology and remediation of land contaminated by agricultural drainage sediment rich in selenium. *Ecotoxicol. Environ. Saf.* **2004**, *57*, 257-269.
- Barabás, N.; Goovaerts, P.; Adriaens, P. Geostatistical assessment and validation of uncertainty for three-dimensional dioxin data from sediments in an estuarine river. *Environ. Sci. Technol.* **2001**, *35*, 3294-3301.
- Leenaers, H.; Okx, J. P.; Burrough, P. A. Comparison of Spatial Prediction Methods for Mapping Floodplain Soil Pollution. *Catena* **1990**, *17*, 535-550.
- French, J. R.; Spencer, T.; Murray, A. L.; Arnold, N. S. Geostatistical Analysis of Sediment Deposition in two small tidal wetlands, Norfolk, UK. *J. Coastal Res.* **1995**, *11*, 308-321.
- Kravchenko, A.; Bullock, D. G. A comparative study of interpolation methods for mapping soil properties. *Agron. J.* **1999**, *91*, 393-400.
- Butcher, J. B. Co-kriging to incorporate screening data: Hudson River sediment PCBs. *Water Resour. Bull.* **1996**, *32*, 349-356.
- Little, L. S.; Edwards, D.; Porter, D. E. Kriging in estuaries: As the crow flies, or as the fish swims. *J. Exp. Mar. Biol. Ecol.* **1997**, *213*, 1-11.
- Burrough, P. A.; McDonnell, R. A. *Principals of Geographical Information Systems*; Oxford University Press: New York, 1998.
- Chiles, J. P.; Delfiner P. *Geostatistics: Modeling Spatial Uncertainty*; John Wiley and Sons: New York, 1999.
- Western, A. W.; Bloschl, G. On the spatial scaling of soil moisture. *J. Hydrol.* **1999**, *217*, 203-224.
- Pardo-Igúzquiza, E.; Chica-Olmo, M.; Atkinson, P. M. Down-scaling cokriging for image sharpening. *Remote Sens. Environ.* **2006**, *102*, 86-98.

- (13) Michalak, A. M.; Kitanidis, P. K. Estimation of historical groundwater contaminant distribution using the adjoint state method applied to geostatistical inverse modeling. *Water Resour. Res.* **2004**, *40*, W08302.
- (14) Sun, A. Y. A robust geostatistical approach to contaminant source identification. *Water Resour. Res.* **2007**, *43*, W02418.
- (15) Snodgrass, M. F.; Kitanidis, P. K. A geostatistical approach to contaminant source identification. *Water Resour. Res.* **1997**, *33*, 537–546.
- (16) Yeh, T. C. J.; Zhang, J. Q. A geostatistical inverse method for variably saturated flow in the vadose zone. *Water Resour. Res.* **1996**, *32*, 2757–2766.
- (17) Zimmerman, D. A.; et al. A comparison of seven geostatistically based inverse approaches to estimate transmissivities for modeling advective transport by groundwater flow. *Water Resour. Res.* **1998**, *34*, 1373–1413.
- (18) Fienen, M. N.; Kitanidis, P. K.; Watson, D.; Jardine, P. An application of Bayesian inverse methods to vertical deconvolution of hydraulic conductivity in a heterogeneous aquifer at Oak Ridge National Laboratory. *Math. Geol.* **2004**, *36*, 101–126.
- (19) Kyriakidis, P. C. A geostatistical framework for area-to-point spatial interpolation. *Geophys. Anal.* **2004**, *36*, 259–289.
- (20) Michalak, A. M.; Bruhwiler, L.; Tans, P. P. A geostatistical approach to surface flux estimation of atmospheric trace gases. *J. Geophys. Res.* **2004**, *109*, D14109.
- (21) Kitanidis, P. K. Quasi-Linear Geostatistical Theory for Inversing. *Water Resour. Res.* **1995**, *31*, 2411–2419.
- (22) Kitanidis, P. K. *Introduction to Geostatistics: Applications to Hydrogeology*; Cambridge University Press: New York, 1997.
- (23) Bogaert, P.; Russo, D. Optimal spatial sampling design for the estimation of the variogram based on a least squares approach. *Water Resour. Res.* **1999**, *35*, 1275–1289.
- (24) Kitanidis, P. K.; Lane, R. W. Maximum-likelihood parameter-estimation of hydrologic spatial processes by the Gauss-Newton method. *J. Hydrol.* **1985**, *79*, 53–71.
- (25) Pannone, M.; Kitanidis, P. K. Large-time spatial covariance of concentration of conservative solute and application to the Cape Cod tracer test. *Transp. Porous Media* **2001**, *42*, 109–132.
- (26) Michalak, A. M.; Hirsch, A.; Bruhwiler, L.; Gurney, K. R.; Peters, W.; Tans, P. P. Maximum likelihood estimation of covariance parameters for Bayesian atmospheric trace gas surface flux inversions. *J. Geophys. Res.* **2005**, *110*, D24107.
- (27) Schabenberger, O.; Gotway C. A. *Statistical Methods for Spatial Data Analysis*; Chapman & Hall/CRC: Boca Raton, FL, 2005.
- (28) U. S. Environmental Protection Agency (EPA). Superfund Site Information Search; 2002; <http://www.epa.gov/superfund/sites/query/basic.htm>; accessed Nov. 2002.
- (29) National Oceanic and Atmospheric Administration/National Ocean Service, Office of Response and Restoration (NOAA). Watershed Database and Mapping Projects; 2002; <http://response.restoration.noaa.gov/cpr/watershed/watershedtools.html>; accessed Nov. 2002.
- (30) Schumacher, B. A. *Methods for the Determination of Total Organic Carbon (TOC) in Soils and Sediments*; Ecological Risk Assessment Support Center, U.S. EPA: Washington, DC, 2002.
- (31) Michalak, A. M. A Gibbs sampler for inequality-constrained geostatistical interpolation and inverse modeling. *Water Resour. Res.* **2008**, *44*, W09437.

ES901431Y